Journal of the Brazilian Society of Mechanical Sciences and Engineering (2022) 44:8
https://doi.org/10.1007/s40430-021-03305-w

TECHNICAL PAPER

Temperature profile and gas emissions of jet fuel using a low power flameless combustor

Jean Andrade Barbosa[1] · José Carlos de Andrade[1] · Fernando de Souza Costa[1] · Christian Jeremi Rodriguez Coronado[2] · Cláudia Gonçalves de Azevedo[3] · Ricardo Amaral de Andrade[1]

Received: 4 January 2021 / Accepted: 25 November 2021

Abstract

Flameless combustion has significant potential for aeronautical applications since it is a regime with homogeneous temperature distribution, relatively low temperatures, high thermal efficiency, reduced NOx emissions, and reduced thermal stress in the chamber. This work demonstrates the possibility of achieving flameless combustion of Jet A-1 fuel and presents experimental data obtained in a small combustion chamber that uses the energy generated to heat up the combustion air with a thermal input of 4.36 kW. A blurry injector was adopted for efficient fuel atomization (Sauter mean diameter of 28.6 ± 0.28 µm) adjacent to the nozzle orifice exit. The evolution of the main process parameters has indicated transition from conventional combustion to flameless regime after 60 min from ignition, with excess combustion air of 70%, fuel mass flow rate of 0.1018 g/s and combustion air temperature 589 K. Combustion air momentum rate and velocity were 0.1678 N and 345 m/s, respectively, whereas the droplet vaporization time was estimated as 0.27 ms and residence time of 3.37 ms. Temperatures measured at different locations inside the chamber were within 987 ± 29.5 K after 75 min from ignition, and average NOx, UHC emissions were, respectively, 21.5 ppm and 1 ppm between 70 and 100 min from ignition and an increase of 20 ppm for CO emission.

Keywords Flameless · Jet fuel · Combustion · Flow blurry · Thermodynamics

List of symbols

A	Nozzle exit area (m^2)
ALR	Air liquid mass ratio (kg/kg)
B_v	Vaporization transfer number (–)
$c_{p,g}$	Gas-phase specific heat (J/kgK)
D_0	Average droplet initial diameter (m)
$D_{0.1}$	Droplet diameter at 10% cumulative mass (m)
$D_{0.5}$	Droplet diameter at 50% cumulative mass (m)
$D_{0.9}$	Droplet diameter at 90% cumulative mass (m)
h_v	Latent heat of vaporization (J/kg)
h_v	Latent heat of vaporization (J/kg)
K_{vap}	Vaporization constant (m^2/s)
k_g	Gas thermal conductivity (W/mK)
$\dot{m}_{air}$	Mass flow rate of combustion air (g/s)
$\dot{m}_l$	Mass flow rate of fuel (g/s)
$\dot{m}_g$	Mass flow rate of gas (g/s)
$\dot{m}_{prod}$	Mass flow rate of products (g/s)
M	Inlet momentum rate (N)
s	Span of droplet size distribution (–)
T_∞	Average chamber temperature (K)
T_s	Droplet surface temperature (K)
$\overline{T}$	Average temperature nearby the droplet surface (K)
t_r	Residence time (s)
t_{vap}	Vaporization time (ms)
v	Droplet exit axial velocity (m/s)
v_{CA}	Combustion air velocity (m/s)
ρ_g	Gas density (kg/m^3)
ρ_l	Fuel density (kg/m^3)
ρ_{mix}	Gas mixture density (kg/m^3)

Technical Editor: Mario Eduardo Santos Martins.

✉ José Carlos de Andrade
jose.andrade@inpe.br

[1] Combustion and Propulsion Laboratory, National Space Research Institute, Cachoeira Paulista, SP 12630000, Brazil

[2] Federal University of Itajubá – UNIFEI, Mechanical Engineering Institute – IEM, BPS Ave.1303, Itajubá, MG 37500903, Brazil

[3] São Paulo State University – UNESP, Campus of Rosana, Barrageiros Ave. 1881, Rosana, SP 19274000, Brazil

Published online: 07 December 2021

1 Introduction

New high efficiency combustion processes with lower pollutant emissions have been investigated along the last decades. This has been accomplished through advanced combustion technologies or advanced alternatives fuels. Since the 1970s, the characteristics of flameless combustion [1] have been described as high recirculation of combustion products, homogeneous temperature distribution, relatively low combustion temperatures, reduced pollutant emissions, high thermal efficiency and reduced thermal stress in the combustion chamber in comparison with conventional combustion processes [2, 3].

There was adopted different acronyms for flameless combustion, e.g., Flameless Oxidation (FLOX), HiTAC (high temperature air combustion), Excess Enthalpy Combustion (EEC), MILD (moderate or intense low oxygen diffusion) combustion or CDC (colorless distributed combustion) [4–8]. All cases are characterized by high temperature oxidizers that are used together with the recirculation of exhaust gases at high turbulence level, and typically, there is no visible flame, with a very lean and stable reaction.

Flameless combustion has a significant potential in the aeronautical industry because of gas turbine paradigm. The higher the temperature, the higher is the turbine efficiency, and the lower is CO emission, but NOx emission raises [1]. This emissions variation is gradual, and it is possible to discover an optimal operating range in which both emissions are low. Usually a temperature between 1000 and 2500 K is satisfactory [9]. Therefore, flameless combustion regime attends this demand because it operates in temperature up to 1200 K with very low CO and NOx emissions, reaching values under 10 ppm under certain operating conditions [9].

Research and development in flameless combustion on aeronautical sector are required because of its great potential [8]. The challenge of making flameless combustion of liquid fuels remains in the fact that the fuel needs to be well vaporized when combustion takes place. This condition adds more variables to be solved during the combustion chamber construction. Some efforts in achieving liquid fuel flameless combustion with different combustors types were made.

Reddy et al. [10], used a two-stage combustor, with kerosene as a fuel and obtained low emissions. In another study, [11] they used a single-stage combustor and obtained the optimum performance to be used both in industry and gas turbines. In both studies, the combustor is initially ignited with a spark plug and a mixture of liquefied petroleum gas (LGP)/air to ensure initial flame stability. Derudi M. and Rota R. [3] used a dual-nozzle laboratory-scale burner to investigate flameless combustion stability of liquid hydrocarbons and obtained results similar to the flameless regime of gaseous fuels. Ye et al. [12] carried out flameless combustion of ethanol, acetone and n-heptane in a reverse flow combustor at pressures of 1–5 bar. They concluded that CO emissions do not depend on pressure, while NOx emissions increased with pressure. Recently, Derudi M. and Rota R. [13] studied the stability of flameless combustion of oxygenated hydrocarbons in a dual-nozzle-scale laboratory burner, and notice that the injection of liquid fuel spray at high velocity allowed the maintenance of flameless conditions. The same condition was reached using gaseous fuel. They affirm that flameless combustion is quite versatile and can create an environment with reduced gas emissions pollutants.

Guillou et al. [14] studied the flameless combustion of propane, n-butane and Jet A. The condition of work was an equivalence ratio of 0.25–0.75 and oxidant temperature greater than 600 K. They stated that, besides n-butane, the other fuels had similar behavior and the flameless regime only occurred with a minimum temperature of 1073 K. Cameretti et al. [15], compared the combustion of ethanol with jet fuel combustion in a gas microturbine concluding that in terms of combustion efficiency are similar, and that NOx emissions were low due to the reduced flame temperature. Cui et al. [16] studied how to perform flameless combustion of liquid fuels and concluded that preheating the combustion air is not an essential factor to carry out such regime. Air injection velocity and exhaust gas mixture are more important factors in the reaction rate control.

Ellis et al. [17] studied emission and soot behavior of liquid biofuels in a process called Power, Water Extraction, and Refrigeration system (PoWER). They demonstrated that flameless combustion can be used in long-term operating systems resulting in low emissions, and that it is possible to take advantage of biomass resources in bio-fuel processing plants. Torresi et al. [18] experimentally and numerically simulated MILD combustion of Diesel in a staged swirled burner showing that this burner can achieve this type of combustion.

Melo et al. [19] describe a combustor model with different nozzles configurations that mix combustion products with inlet air, which generates a large recirculation zone in the combustion chamber. Concluding that the recirculation rate is a function of the nozzle geometry. Also, that the air inlet configuration influences the combustion efficiency. Cha et al. [20] used a two-stage combustor, which the first stage consists in a premixed burner and affirmed that the increase in burnt gas velocity of the first stage results in a lower spatially uniform temperature together with emissions reduction.

This work is a continuation of Azevedo et al. [21], with the following differences: focus on flameless combustion

using jet fuel and different combustion air heating system (a parameter required to achieve flameless combustion regime). Therefore, the main contribution of this work is the new combustor configuration (described in the next section).

This manuscript initially describes the combustor configuration that operates with a power input of 4.36 ± 0.005 kW. The preheating of the combustion air is realized through the chamber walls. Fuel atomization is made by a blurry injector with high atomization efficiency that generate relatively small droplets just after the nozzle orifice exit. Flameless regime is characterized by measurements of the main parameters of the combustion process, such as temperatures, flow rates and emissions of NOx, CO, CO_2 and UHC (unburned hydrocarbons).

2 Experimental setup

2.1 Blurry injector

"Flow blurring" is a twin fluid atomization process that exploits the advantages of internal and external mixing. It has several advantages over other injection techniques, such as formation of a relatively uniform spray, robustness, high atomization efficiency, and excellent fuel vaporization [22]. Blurry injector generates a fine and uniform spray at lower pressures in contrast to effervescent, air blast and pressure injectors that needs higher pressures. [23]. Specifically, the flow blurring injector is ten times more efficient than an air blast atomizer [24]. The result of this efficiency is a cleaner combustion of fossil fuels because of the better mixing with air, resulting in a more efficient combustion [24–26].

Blurry injector was used in this work because it operates in low pressure compared to other injectors. This low-pressure condition results in a relative low fuel injection velocity, which is essential to the small combustion chamber. In a higher fuel inlet velocity, the droplet does not burn completely, resulting in an inefficient combustion. Also, the injector was designed and built to operate in optimal condition in the combustion chamber of this work.

A blurry injector has two concentric cylindrical tubes, and a downstream orifice plate, as shown in Fig. 1. The liquid fuel is fed through the inner tube, while the atomization air is supplied through the external tube. The exit injector orifice diameter is 0.5 mm, and is equal to the exit fuel tube diameter. The fuel tube tip is located at 0.125 mm away from the injector exit orifice in order to produce the blurry effect. Fuel and atomization air mix within the injector before leaving the orifice plate, producing the spray downstream [21].

The air/liquid mass ratio (ALR) is a relevant operational parameter of the injector because, for a given liquid mass flow rate and corresponding power input, it will determine the air mass flow rate and the spray characteristics.

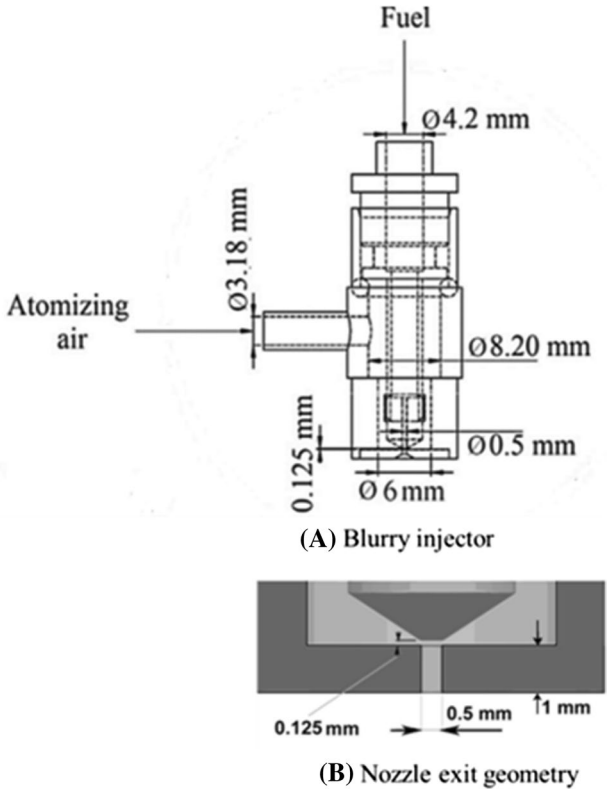

Fig. 1 **a** Schematic of the blurry injector; **b** Nozzle exit geometry [21]

2.2 Combustion chamber

The experimental setups used in other works about flameless combustion of liquid fuels are described next. Figure 2 presents the different types of combustion chamber utilized in previous works. Reddy et al. [10] used a two-stage combustor, as shown in Fig. 2a, in which injects fuel with a pressure-swirl injector, and the combustor is initially ignited by a spark plug, and then maintained by a mixture of LGP-air. In their other work [11], the combustion chamber had only one stage and a rounded shape at the top (Fig. 2b). Figure 2c shows the combustion chamber of Ye et al. [12], which uses a reverse-flow MILD combustor that contains two chambers: one for ignition and the other is the main chamber. It was used an external recuperator for the combustion air heating, and the fuel is vaporized before entering the chamber. Recently, Derudi and Rota [13] assembled a combustion chamber (Fig. 2d) that can be operated with either liquid or gaseous fuel by heating the combustion air through an electric oven placed around the combustion chamber.

The test bench in this work comprises: a combustion chamber, chamber support, pressurizer tanks, fuel tank, air compressor, temperature and pressure transducers, control valves, data logger, gas analyzers, and other devices, as shown in Fig. 3.

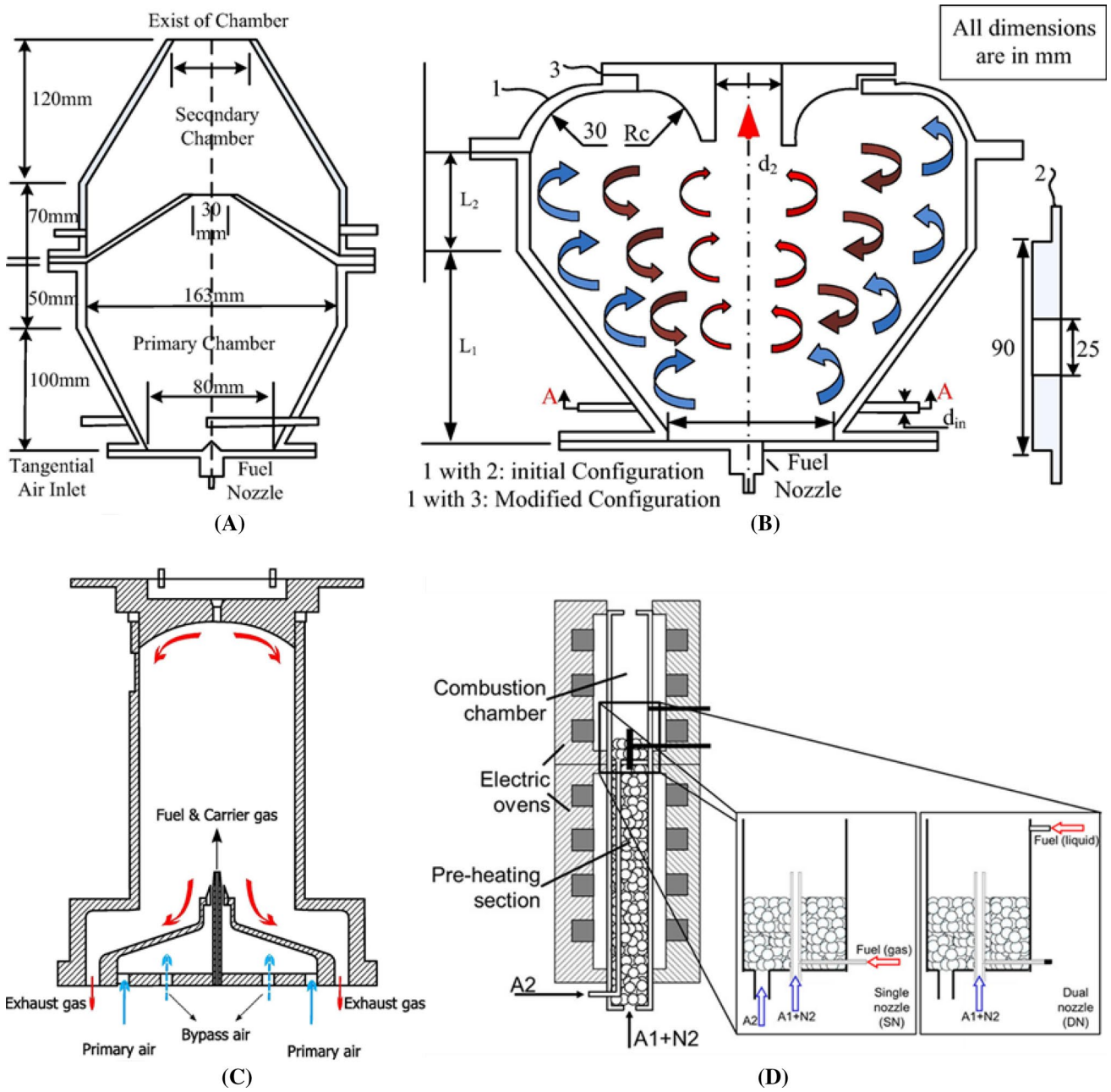

Fig. 2 Different types of combustion chamber, **a** Reddy et al. [10], **b** Reddy et al. [11], **c** Ye et al. [12], **d**—Derudi and Rota [13][3]

The combustion chamber is a 316 stainless steel cylinder of 500 mm length and 101 mm internal diameter. Also, has a ROBAX® ceramic glass window (35 × 200 × 5 mm) for optical access. The combustion chamber scheme is presented in Fig. 4.

The differences of the combustion chamber of this work and the other studies mentioned above are: cylindrical shape (simpler to be built); electric ignition using a spark plug; the heating of the combustion air that is achieved with the heat generated in the combustion chamber itself, through a 1/4" diameter stainless steel serpentine placed around the chamber. The stainless steel serpentine is a difference between this work and the experimental setup of Azevedo et al., [21].

Temperatures in the chamber were determined by K-type mineral insulated thermocouples (diameter 1.5 mm), with maximum measured temperature of 1573 K (accuracy ± 0.1%). Seven thermocouples were placed 60 mm apart along the combustion chamber at three different radii: 5, 20 and 35 mm. Additionally, a thermocouple was placed at the chamber bottom to measure inlet combustion air temperature, and another thermocouple was placed at the top of the

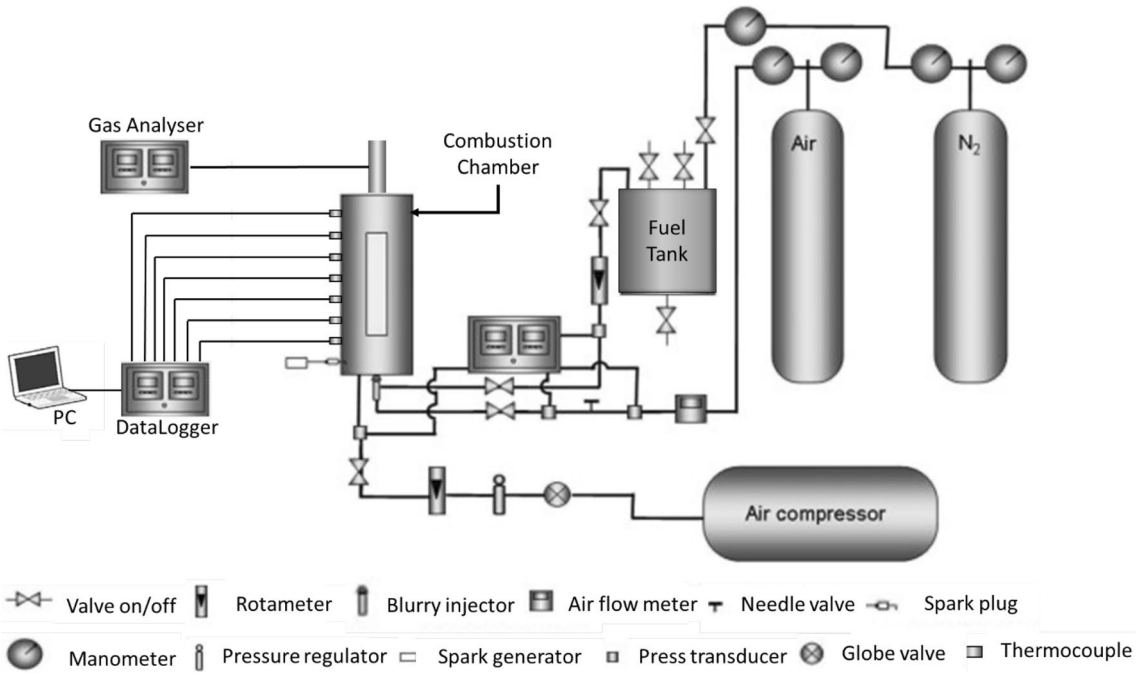

Fig. 3 Test workbench scheme [21]

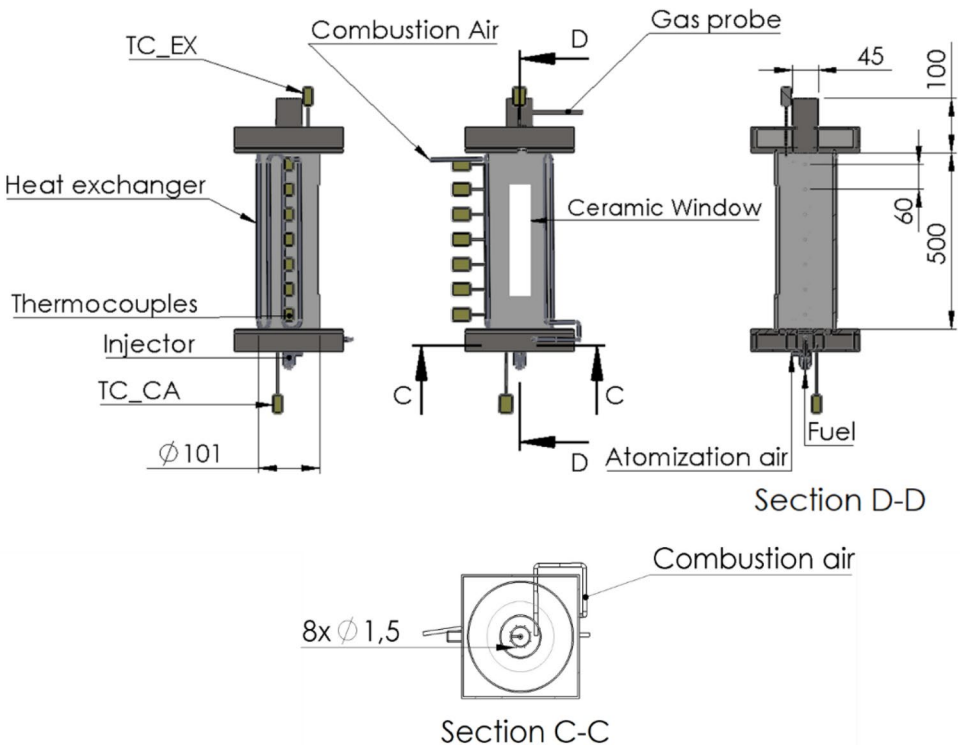

Fig. 4 Combustion chamber scheme

chamber to measure exhaust gas temperature. The chamber was insulated with a ceramic thermal blanket to minimize heat losses to ambient.

The combustion chamber has an injection plate with a blurry injector along the axis. Six holes with diameter 1.5 mm, and equally spaced at 20 mm radius are used for injection of combustion air parallel to fuel spray. Exhaust gas was removed through a 45 mm diameter and 100 mm length duct on the combustion chamber top. It was placed a probe at the exit duct to sample the exhaust gas to the

gas analyzers. An ignition system with an electric spark of 450 W was placed near the injector exit nozzle.

The combustion air was supplied by a 32 HP Schulz air compressor, nitrogen was used as fuel pressurizer, and synthetic air was supplied to the blurry injector. Continuous measurements of temperatures and sample gas composition were carried out during tests. Flue gas composition samples were withdrawn at the exhaust duct using a water-cooled iso-kinetic stainless-steel probe. Table 1 presents the range and uncertainty of all measuring instruments.

To achieve flameless combustion the fuel is electrically ignited, and a conventional flame regime is established with a stoichiometric relationship. Then, the heat generated by these initial burning, heats the combustion air, through the combustion chamber walls. Once the combustion air temperature is above the autoignition of the tested fuel, the combustion air flow is increased to an over-rate, until the flameless combustion regime is reached. The experiment shows that once the flameless regime is achieved in this system, it lasts for an unlimited time.

3 Results and discussions

3.1 Characterization of the spray

The injector is a significant factor in the combustion of liquid fuels. The injector must produce an excellent atomization to successfully vaporize and mix the fuel with oxidant. For this purpose, a blurry injector was chosen, as mentioned before. In order to characterize the spray formed by the injector, it is necessary to detail some operation parameters: ALR, injection pressure, fuel mass flow rate, Sauter mean diameter (SMD), droplet size distribution and spray cone angle. These parameters act together in the injector operation. Table 2 presents the injector operating parameters.

The higher the ALR, the better is the atomization. However, there is an optimum point that above this there is no improvement in atomization [27]. In this work the optimum ALR is 0.064. The uncertainty of the ALR is given by the square root of the sum of the squares of the uncertainties of the mass flow rates of air and fuel. The ALR uncertainty is ± 0.003.

Table 2 Injector parameters

ALR (kg/kg)	0.064
Pressure injection (bar)	1.52
Fuel mass flow rate (g/s)	0.1018
SMD (μm)	28.6
Span (–)	5.35
Spray cone angle (°)	15.39

SMD, droplet size distribution and span were measured by a Malvern Spraytech ©, which uses a laser diffraction system with accuracy of $\pm 1\%$, full scale. These measures were taken at 45 mm below the injector exit along the centerline of the cone angle. The blurry injector provides a spray with Sauter mean diameter (SMD) of 28.6 μm and span $s = (D_{0.9} - D_{0.1})/D_{0.5}$, where $D_{0.1}$, $D_{0.5}$ and $D_{0.9}$ are the droplet diameters at 10%, 50%, and 90% cumulative masses, respectively. Low SMD and low span represent a uniform spray with small droplets. Another parameter that indicates a uniform droplet spray is the droplet size distribution which is presented in Fig. 5. It is possible to observe that the distribution of droplets in the spray is uniform, with its greatest concentration around the SMD.

Figure 6 shows the cone angle of the spray formed by the injector, measured digitally for the working condition. The value of the cone angle was 15.39 °. Small angles ($< 60°$) promote greater penetration of the spray in the environment because of the high component of axial velocity. On the other hand, the high axial velocity maintains the flame further of the injector outlet, and this may cause combustion instability [28]. This work had no

Table 1 Range and uncertainty of the measuring instruments

Parameters	Measure instrument	Ranges	Accuracy*
Atomization air mass flow rate	Rotameter (GFM 1109)	0–5 l/min	±1.5%
Combustion air mass flow rate	Rotameter (Omel model N)	7.5–75 l/min	±2%
Fuel mass flow rate	Rotameter (Omel model 3P)	0.05–0.5 l/min	±5%
Temperature	K-type thermocouple	0–1260 °C	±0.1%
Injector Pressure	Pressure transducer	0–20 bar	±0.5%
O_2 concentration	Paramagnetic analyzer	0–25%	±0.5%
CO concentration	Non-dispersive infrared gas analyzer	0–15%	±0.5%
CO_2 concentration	Non-dispersive infrared gas analyzer	0–20%	±0.5%
NOx concentration	Chemiluminescence analyzer	0–5000 ppm	±3%
UHC concentration	Flame ionization detector	0–20,000 ppm	±3%

*The accuracy is in full range

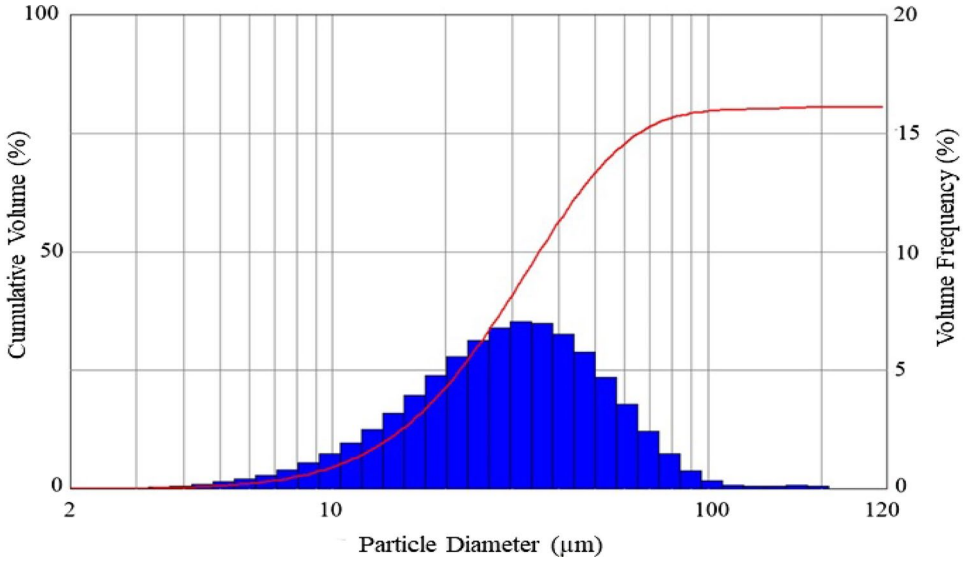

Fig. 5 Droplet size distribution of the spray

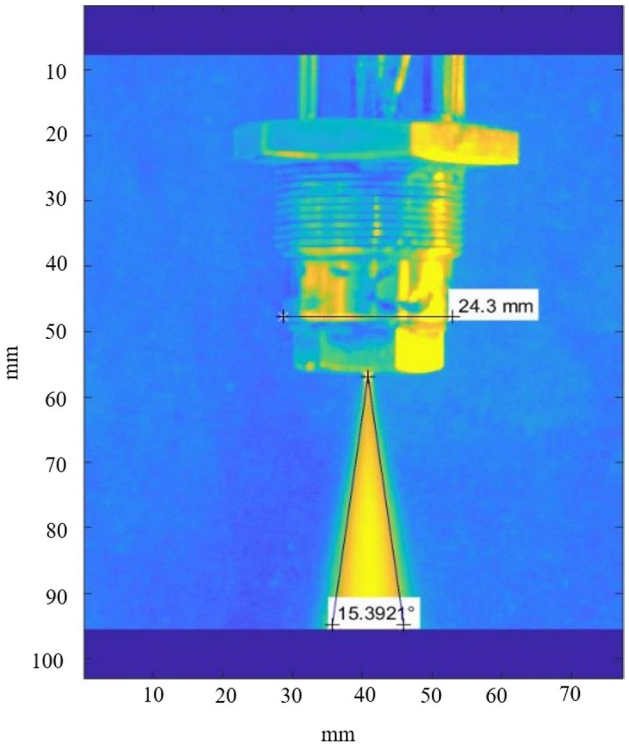

Fig. 6 Spray cone angle

stability problem because the average velocity of droplets is small in relation to the velocity of the combustion air.

The average droplet velocity was estimated considering that the spray cone angle is relatively small, and that droplets are formed adjacent to the injector nozzle exit. Since the droplets are relatively small, their average velocity can be assumed equal to the average gas velocity. An equation for the nozzle exits velocity (v) is derived in Appendix A:

Table 3 Main test parameters

Volumetric flow rate of combustion air (L/min)	70
Equivalence ratio (–)	0.5
Air combustion velocity (m/s)	345.68
Inlet momentum rate (N)	0.1714
Power thermal input (kW)	4.36

$$v = \frac{\dot{m}_l}{A}\left(\frac{1}{\rho_l} + \frac{ALR}{\rho_g}\right) \quad (1)$$

where $\dot{m}_l$ is the fuel mass flow rate, A is the nozzle exit area, ρ_l and ρ_g are the liquid and gas (air) densities, respectively.

3.2 Test conditions

Tests were performed at ambient pressure. Table 3 summarizes the test conditions in the flameless regime and the main test parameters, while Table 4 presents important fuel characteristics [29, 30]. Preliminary tests were required to determine the optimum conditions to achieve the flameless combustion regime. A preheating period of 60 min in the flaming regime, with combustion air flow rate of 50 L/min and fuel mass flow rate of 0.1018 g/s, was required to heat up the combustion air and the chamber walls. The combustion air flow rate was increased to 70 L/min at 60 min from ignition in order to reach the flameless regime, yielding an excess air of 70%. However, the fuel flow rates and the atomization conditions were kept the same in both regimes. Blow off would occur if larger fuel flow rates were used. The combustion air flow rate was limited by the heat transfer in the ¼" serpentine heat exchanger and by the rotameter operational range.

Table 4 Physicochemical properties of Jet A-1 fuel [29]

Chemical formula	$C_{11}H_{21}$ [30]
Initial boiling point	423 K
Flash point	313 K
Lower flammability limit (298 K)	0.7% Vol
Upper flammability limit (298 K)	5.0% Vol
Vapor pressure (273 K)	0.480 mmHg
Density (298 K)	804 kg/m^3
Self-ignition temperature	483 K
Freezing point	226 K
Kinematic viscosity (313 K)	1 – 2.4 mm^2/s
LHV (MJ/kg)	42.8

Air momentum, residence and vaporization times are important parameters to achieve flameless combustion. The first one promotes entrainment and recirculation that increases the mixture inside the chamber, reducing the concentration of oxygen in the flame region, a necessary condition for the flameless combustion regime [31–33]. For the calculation of the inlet momentum rate in the combustion chamber will be considered only longitudinal direction. Considering steady state flow, incompressible fluid, inviscid, no body forces and no pressure variation. Also, it is considered that the injector fuel and air have the same velocity. Therefore, from Navier–Stokes equations the inlet momentum rate in longitudinal direction of the combustion chamber can be calculated by:

$$M = (\dot{m}_l + \dot{m}_g)v + \dot{m}_{air}v_{CA} \tag{2}$$

where $\dot{m}_l, \dot{m}_g$ and $\dot{m}_{air}$ are the fuel mass flow rate, atomization gas mass flow rate and combustion air mass flow rate, respectively; v is the average droplet velocity, and v_{CA} is the combustion air velocity. The first term represents the injector momentum rate, and second term represents the air combustion momentum rate. In this work, inlet momentum rate was 0.1715 N, injector momentum rate was 0.0037 N and air combustion momentum rate was 0.1678 N. Consequently, the combustion air presents a momentum rate about 46 times larger than both liquid fuel and atomization air.

The combustor residence time (t_r) is comprised of the following times: vaporization, recirculation, mixing and chemical. According to Reddy et al. [11], the increase in residence time increases flame stability and recirculation rate. Kruse S. et al. [34], affirm that NOx emissions increases linearly, and that CO emissions reduces when the residence time is longer. On the other hand, Khalil and Gupta [35] claim that a shorter residence time can cause a slight increase in CO emission. Residence time in the combustor was estimated as $t_r = \rho_{mix}V/\dot{m}_{prod}$. The gas mixture density ρ_{mix} can be calculated by CEA NASA (assuming T = 1000 K and p = 1 bar, with no heat losses). For this work, the estimated residence time was 3.37 ms.

To obtain a uniform burning of liquid fuel, the fuel spray vaporization time must be low [36]. Vaporization time was estimated as $t_{vap} = D_0^2/K_{vap}$ [37], where D_0 = SMD is the average droplet initial diameter (m); K_{vap} is the vaporization constant given by:

$$K_{vap} = \left(\frac{8k_g}{\rho_l c_{p,g}}\right)\ln\left(1 + B_v\right) \tag{3}$$

where ρ_l is the liquid fuel density (kg/m^3), k_g is the gas thermal conductivity, $c_{p,g}$ is the gas-phase specific heat (J/kgK), $B_v = c_{p,g}\left(T_\infty - T_s\right)h_v$ is the vaporization transfer number, and h_v is the latent heat of vaporization (J/kg). T_∞ is the average chamber temperature (K), T_s is the droplet surface temperature, and $\overline{T} = 0.5\left(T_\infty + T_s\right)$ is the average temperature nearby the droplet surface. It was considered that droplets emerge from injector nozzle at boiling point, $T_s \cong T_b$, resulting in a neglected droplet heat-up period. Vaporization time of this test was 0.27 ms. Therefore, once $t_{vap} \ll t_r$, there is complete vaporization of fuel inside the chamber.

3.3 Temperature profile

To perform the transition from conventional combustion to flameless regime, it was necessary to increase air combustion inlet velocity because high air combustion velocity creates gas recirculation in the combustor chamber. This recirculation makes reaction spatially distributed in the entire chamber, consequently a uniform temperature profile.

In preheating time (0 < t < 40 min) the combustion is made in stoichiometric proportion with the velocity 30% smaller than flameless regime that has 70% excess air. Transition from the conventional combustion regime up to flameless combustion regime can be observed in Fig. 7 that shows temperatures inside the chamber measured by thermocouples located at $r = 20$ mm and $x = 60$, 120, 180, 240, 300, 360 and 420 mm. Exhaust gas and combustion air temperatures are also shown. The flameless regime occurs when the measured combustion air temperature (TC_CA) attains about 637 K, above the jet A-1 fuel self-ignition temperature.

Therefore, the rise in temperature at transition mode (40 min < t < 60 min) is due to the increase in chamber temperature. However, to enter the flameless regime, and maintain a uniform temperature profile is necessary a bigger air combustion inlet velocity. This velocity increase rises the recirculation rate, and it starts to form vortexes inside the combustion chamber. Once, the velocity is maintained at a certain value, these vortexes start to distribute the reaction rate to entire combustion chamber uniformizing the temperature profile (t > 70 min), as show in Fig. 7.

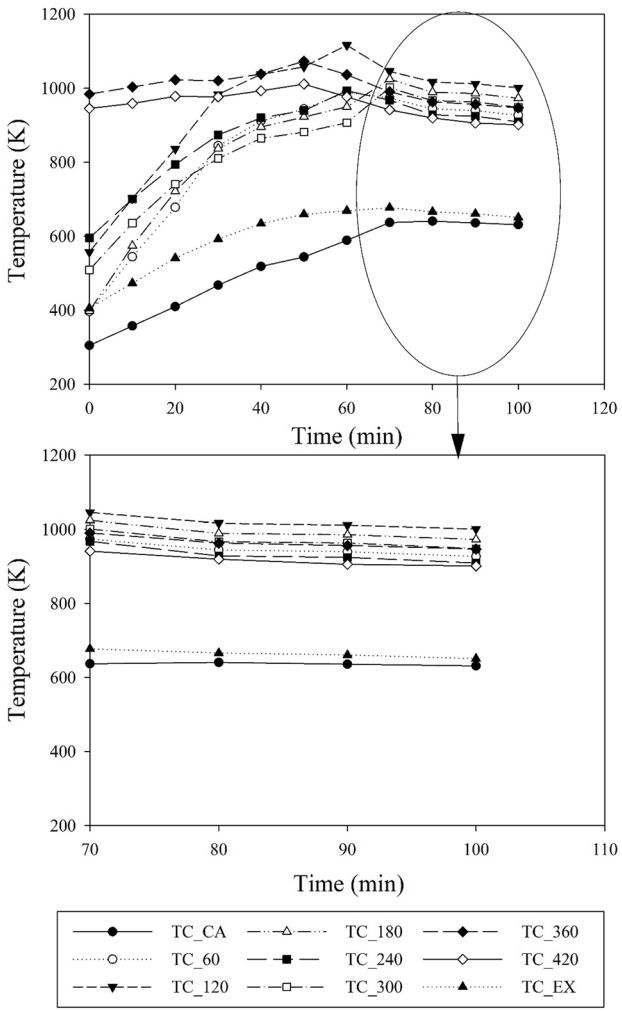

Fig. 7 Temperature evolution at different locations

This statement is verified by temperature measured by the thermocouples TC_360 and TC_420 that are placed at the flame tip of conventional combustion. In preheating and transition mode, the temperature of both thermocouple is maintained approximated at 1000 K and the temperature of the other thermocouples, eliminating TC_CA and TC_EX that are not placed at the reaction zone, tends to flame tip temperature showing that the reaction rate, consequently temperature profile, is becoming uniform in the combustor chamber.

The maximum temperature inside the combustion chamber was 1019 K, and the minimum was 916 K. Taking out the air combustion temperature and exhaust gas temperature, the combustion chamber yielded an average value of 967.5 K. Variations of temperature in all thermocouples inside the chamber stay below 60 K from 70 to 100 min after ignition showing a good temperature uniformity at the thermocouple positions considered. Exhaust gas temperatures, measured by the TC_EX thermocouple, attain 677 K, and

Table 5 Temperature range measure at flameless regime with $r = 20$ mm

Thermocouple	Lowest T (K)	Highest T (K)
TC_CA	631.28	640.64
TC_60	926.91	973.65
TC_120	1001.57	1045.73
TC_180	972.85	1024.66
TC_240	909.15	967.78
TC_300	948.06	1001.25
TC_360	946.9	990.44
TC_420	901.26	941.19
TC_EX	650.98	677.15

the difference of combustion air temperature and exhaust gas temperature is about 40 K, showing efficient heat transfer between combustion air and chamber walls. Table 5 presents the temperature range measure at flameless combustion.

Moreover, it can be concluded that the average temperature on the flameless regime is influenced by the quantity of fuel injected in the combustion chamber. As stated before, the flameless temperature on combustion chamber is defined by the flame tip, higher the fuel concentration in the combustion chamber (thermal input) higher the flame temperature. This relation was also observed by Reddy et al. [11] that performed experiments with different thermal inputs (5.4–21 MW/m^3) with kerosene fuel and claims that the temperature in the chamber is directly proportional to the thermal input. Comparing with this work that has a thermal input of 1.08 MW/m^3 with a maximum temperature of 1019 K with their work (5.4 MW/m^3/1633 K) the proportionality between the thermal input.

In order to make an entire temperature profile, it is necessary to measure the temperature radially in the combustion chamber because the vortexes created by the recirculation can change the temperature in this direction. Figure 8 shows temperatures inside the combustion chamber at $t = 75$ min, during the flameless combustion regime, at positions $r = 5$, 20 and 35 mm and $x = 60$, 120, 180, 240, 300, 360 and 420 mm, with $x = 0$ mm at the injector plate. Table 6 presents the maximum e minimum experimental temperatures.

It is observed a relatively uniform temperature distribution within the combustion chamber, with temperature variation less than 50 K. Temperatures closer to the wall ($r = 35$ mm) are lower than temperatures nearer the longitudinal axis, and there is a slight negative temperature gradient, caused by heat losses along the combustor wall. The heat loss is expected because it is natural of any system. However, the configuration of this work uses this heat loss in the wall to heat up the combustion air trough conduction heat transfer. In this way, there is no necessity of parallel system to heat up the combustion air, in contrary of other

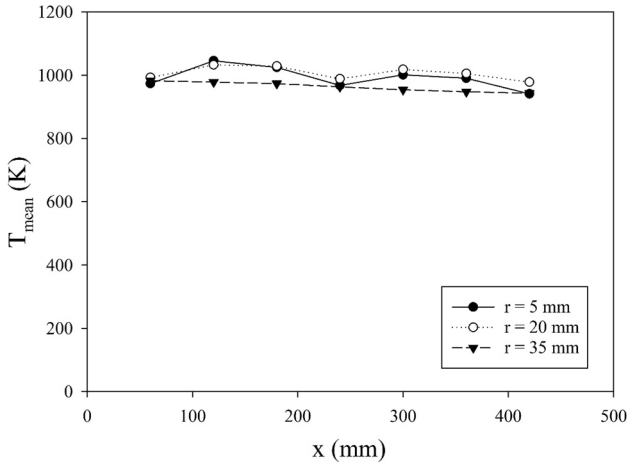

Fig. 8 Temperature distribution during flameless regime at 75 min

Table 6 Measure temperature range at $r = 5$, 20 and 35 mm at 75 min

Thermocouple	$r = 5$ mm	$r = 20$ mm	$r = 35$ mm
TC_60	973.65 K	993 K	983 K
TC_120	1045.73 K	1033 K	978.23 K
TC_180	1024.66 K	1028.85 K	973.52 K
TC_240	967.78 K	988.55 K	963.32 K
TC_300	1001.25 K	1018.26 K	954.25 K
TC_360	990.44 K	1005.48 K	948 K
TC_420	941.19 K	978.25 K	943.5 K

works in the literature [3, 10–13]. In other words, the combustion chamber itself makes the combustion air heat up.

It is observed from Fig. 8 that temperature in $r = 5$ mm and $r = 20$ mm is closely to each other and has the same tendency. At, $x = 60$, 240, 360 mm the average temperatures are 983.32 K, 965.55 K and 942.34 K, respectively, between these lengths there is an increase in the temperature at same radii followed by a decrease. One possible reason for this behavior is that the thermocouples placed in $x = 120$, 180, 300, 360 mm are inside the vortexes created by gas recirculation. Inside, the vortex is excepted a little higher temperature in comparison with other locations of the chamber, due to the gas heat conduction. One possibility for this behavior is that the other thermocouples are placed outside or near the vortex, resulting in a small relative temperature. However, further investigation with numerical simulations, that is not the scope of this work, is necessary to confirm the size shape and location of the vortexes inside the combustion chamber.

Reddy et al. [11] found a radial temperature gradient of 443 K, in contrast to this work, which had a 50 K variation. This shows that the experimental configuration present in this work has greater radially temperature uniformity. Moreover, the measure average temperature is at the same range measured by Derudi and Rota [13].

To qualitative analyze the flameless combustion in this work, pictures taken through the ceramic window are presented in Fig. 9. Figure 9a shows a photo of conventional combustion process, while Fig. 9b presents an image of flameless combustion regime. The visible flame radiation inside the chamber decreased significantly in flameless regime, and the glow of thermocouples could be clearly observed. During conventional combustion, there was significant soot deposition on the ceramic window, reducing flame visibility. As gas recirculation rate increased, and flameless regime was attained, soot formation was significantly decreased, allowing the observation inside the chamber.

3.4 Emissions

The evolution of emissions of UHC, NOx, CO, CO_2 and O_2 during conventional combustion and flameless regimes is shown in Fig. 10. Table 7 presents the range measured of the emission.

Concentration of unburned hydrocarbon (UHC) decreases significantly over time, from approximately 30 ppm to around 1 ppm in 20 min, in the flaming period, due to the transition from stoichiometry to lean combustion. After that, it remains at about 1 ppm in the flameless regime, due to the high excess air. O_2 concentration increases from about 6.8% at beginning, to around 10.5% at $70 < t < 100$ min, due to increase in combustion air flow

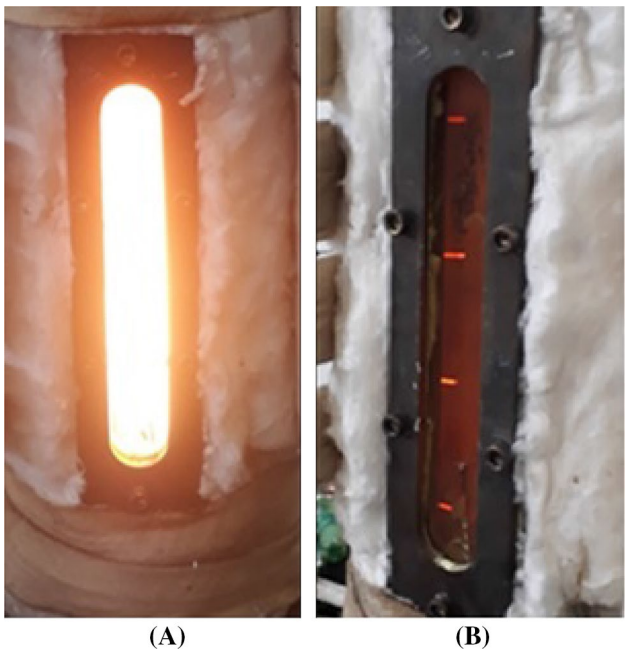

Fig. 9 **a** Conventional combustion regime; **b** Flameless combustion regime

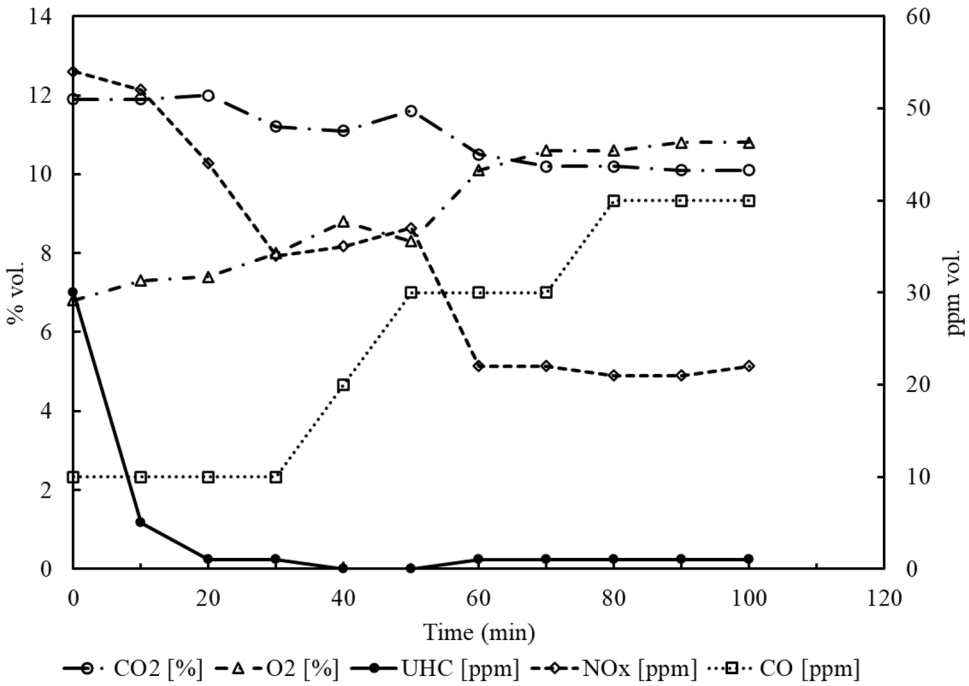

Fig. 10 Evolution of CO_2, O_2, UHC, CO and NOx emissions

Table 7 Emissions range measurements at flameless regime

Gas	Lowest concentration	Highest concentration
CO_2 (%)	10.1	10.5
O_2 (%)	10.1	10.6
UHC (ppm)	1	–
CO (ppm)	30	40
NOx (ppm)	21	22

rates at about $t = 50$ min. Air flow rates remain constant during the flameless combustion regime from $t = 70$ min to 100 min. CO_2 concentration decreases from about 11.5% during the flaming regime to approximately 10.2% in the flameless regime, probably, because of the increase in CO concentration.

NOx concentration decreases from 54 to 34 ppm between 0 and 30 min. Then, it increases slightly up to 37 ppm at 50 min and then decreases to about 22 ppm in the flameless combustion regime between 70 and 100 min. NOx was not formed by the thermal mechanism during the flameless combustion regime, since the average combustion chamber temperature was 993 K. These results are in accordance with another experiments in the literature [3, 10, 11, 13]. In all of them, NOx emissions decreased in flameless combustion regime.

CO emission remains approximately constant at 10 ppm from 0 to 30 min, increases linearly up to 30 ppm from 30 to 50 min, remains constant at 30 ppm from 50 to 70 min, goes up from 30 to 40 ppm between 70 and 80 min, and finally remains constant at 40 ppm from 80 to 100 min.

It was observed an increase in CO emissions when the combustion entered in flameless regime. This work has a lower average temperature inside the combustion chamber when compared to other works in the literature that uses jet fuel [3, 11, 13]. The increase in CO formation can be explained by the reaction $OH + CO \leftrightarrow H + CO_2$ that controls the flameless combustion reaction [38]. A lower maximum temperature reduces the OH concentration, consequently raises CO formation, with respect to conventional combustion. This statement is confirmed by [39, 40]. In addition, Tu et al. [40] state that a higher temperature between 1073 and 1273 K can reduce the CO emission. Therefore, it can be concluded that one of the reasons for the increase in CO concentration is due to the low average temperature inside the combustion chamber during the flameless regime.

In other hand, Cavigiolo et al. [41] found a temporary peak in CO formation when the recirculation rate is around 3. In this work, the rate of recirculation was not calculated because of combustor geometry. Equivalence ratio is another factor that influenced the CO formation. The equivalence ratio of this work is 0.5 and the CO emission in flameless regime was 40 ppm, in concordance with previously cited works [3, 10, 11, 13, 35].

4 Conclusions

Jet A-1 fuel flameless combustion was achieved within a small combustion chamber that uses energy generated within to heat up the combustion air. The liquid fuel was fully atomized just at the exit orifice of a blurry injector, forming a relatively uniform spray with SMD of 28 mμ and low droplet size span (5.35). The combustion air velocity and momentum rate were, respectively, 345 m/s and 0.1678 N, and the time required to reach flameless regime was about 70 min with an equivalence ratio of 0.5. Temperatures inside the combustion chamber varied from 916 to 1019 K in the flameless regime, with combustion air temperatures varying from 631 to 640 K. Emissions of NOx, UHC, CO and CO_2 were, respectively, 22 ppm, 1 ppm, 40 ppm and 10.2% during the flameless regime. The major finds of this work can be summarized as:

- The cylindrical format of the combustion chamber of this work promotes a sufficient gas recirculation rate, resulting in a uniform temperature profile.
- The radially temperature profile has an increase in x = 120, 180, 300, 360 mm with r = 5 and 20 mm because of the localization of the thermocouples that are inside the vortexes created by the gas recirculation inside the combustion chamber. However, further investigation with numerical simulations is necessary to define the size, shape and location of the vortexes inside the combustion chamber.
- The combustion air heating system used in this work uses the heat generated in the chamber, which reduces extra components in the construction of the combustion chamber. The proposed system presented good efficiency, promoting a heating of approximately 70 min.
- Emissions in general were low, but there was an increase in CO concentration during flameless regime. CO emission increases because of the small average combustor chamber temperature that reduces the OH formation, causing an increasing in CO formation. However, the overall CO emission is in accordance with other studies [3, 10, 11, 13, 35] taking in account the equivalence ratio.

Appendix A

Derivation of the nozzle exit velocity

The exit area of injector, A, is the sum of the areas occupied by gas and liquid, i.e., $A = A_g + A_l$, where subscript g refers to the atomizing gas and subscript l refers to the liquid. Mass flow rates of liquid and air at the injector exit are given, respectively, by $\dot{m}_l = \rho_l A_l v_l$ and $\dot{m}_g = \rho_g A_g v_g$, where ρ is the density and v is the velocity.

Assuming that liquid and gas at the nozzle outlet have equal velocities, $v = v_g = v_l$, then $\dot{m}_l = \rho_l(A - A_g)v$ and $\dot{m}_g = \rho_g A_g v$. Dividing these two mass flow rates, it follows that:

$$\frac{\dot{m}_g}{\dot{m}_l} = \frac{\rho_g A_g}{\rho_l(A - A_g)} \tag{4}$$

Replacing the air–liquid mass ratio $ALR = \dot{m}_g/\dot{m}_l$ in Eq. (1), it yields:

$$A_g = \frac{ALR\rho_l A}{\rho_g + ALR\rho_l} \text{ and } A_l = \frac{\rho_g A}{\rho_g + ALR\rho_l}.$$

The liquid and gas velocity at the injector exit orifice can be calculated from:

$$v = \frac{\dot{m}_l}{\rho_l A_l} = \frac{\dot{m}_l}{A}\left(\frac{1}{\rho_l} + \frac{ALR}{\rho_g}\right)$$

Density of the gas at the injector exit orifice can be estimated by considering the perfect gas equation:

$$\rho_g = P_g/RT_g.$$

If the gas injection pressure is above the critical pressure, i.e.,$P_{g,inj} > P_a((\gamma+1)/2)^{\frac{\gamma}{\gamma-1}}$, where P_a is the ambient pressure and γ is the ratio of the gas specific heats, the gas flow becomes sonic at the nozzle exit orifice. Consequently,

$$P_g = P_{g,inj}\left(\frac{2}{\gamma+1}\right)^{\frac{\gamma}{\gamma-1}} \text{ and } T_g = \frac{2}{\gamma+1}T_{g,inj}, \text{ yielding}$$

$$\rho_g = \frac{P_{g,inj}}{RT_{g,inj}}\left(\frac{2}{\gamma+1}\right)^{\frac{1}{\gamma-1}}$$

If the injection pressures of gas is lower than the critical pressures then $P_g = P_a$ and, for isentropic flow, $T_g = T_{g,inj}\left(P_a/P_{g,inj}\right)^{\frac{\gamma-1}{\gamma}}$, yielding $\rho_g = \frac{P_{g,inj}}{RT_{g,inj}}\left(\frac{P_a}{P_{g,inj}}\right)^{\frac{1}{\gamma}}$.

References

1. Wünning JA, Wünning JG (1997) Flameless oxidation to reduce thermal no-formation. Prog Energy Combust Sci. https://doi.org/10.1016/s0360-1285(97)00006-3
2. Coelho PJ, Peters N (2001) Numerical simulation of a mild combustion burner. Combust Flame. https://doi.org/10.1016/S0010-2180(00)00206-6
3. Derudi M, Rota R (2011) Experimental study of the mild combustion of liquid hydrocarbons. Proc Combust Inst. https://doi.org/10.1016/j.proci.2010.06.120

4. Katsuki M, Hasegawa T (1998) The science and technology of combustion in highly preheated air. In: Symposium (International) on Combustion
5. Tsuji H, Gupta AK, Hasegawa T, et al (2002) High temperature air combustion: From energy conservation to pollution reduction
6. Cavaliere A, Joannon M (2004) Mild Combustion. Prog Energy Combust Sci 30:329–366
7. Arghode VK, Gupta AK (2010) Effect of flow field for colorless distributed combustion (CDC) for gas turbine combustion. Appl Energy. https://doi.org/10.1016/j.apenergy.2009.09.032
8. Xing F, Kumar A, Huang Y et al (2017) Flameless combustion with liquid fuel: a review focusing on fundamentals and gas turbine application. Appl Energy 193:28–51. https://doi.org/10.1016/j.apenergy.2017.02.010
9. Khidr KI, Eldrainy YA, EL-Kassaby MM, (2017) Towards lower gas turbine emissions: Flameless distributed combustion. Renew Sustain Energy Rev 67:1237–1266. https://doi.org/10.1016/j.rser.2016.09.032
10. Mahendra Reddy V, Sawant D, Trivedi D, Kumar S (2013) Studies on a liquid fuel based two stage flameless combustor. Proc Combust Inst. https://doi.org/10.1016/j.proci.2012.06.028
11. Reddy VM, Katoch A, Roberts WL, Kumar S (2015) Experimental and numerical analysis for high intensity swirl based ultra-low emission flameless combustor operating with liquid fuels. Proc Combust Inst. https://doi.org/10.1016/j.proci.2014.05.070
12. Ye J, Medwell PR, Varea E et al (2015) An experimental study on MILD combustion of prevaporised liquid fuels. Appl Energy. https://doi.org/10.1016/j.apenergy.2015.04.019
13. Derudi M, Rota R (2019) 110th Anniversary: MILD Combustion of Liquid Hydrocarbon-Alcohol Blends. Ind Eng Chem Res. https://doi.org/10.1021/acs.iecr.9b02374
14. Guillou E, Cornwell M, Gutmark E (2009) Application of "Flameless" combustion for Gas Turbine Engines. In: 47th AIAA Aerospace Sciences Meeting including the New Horizons Forum and Aerospace Exposition
15. Cameretti MC, Tuccillo R, Reale F, Piazzesi R (2011) Liquid bio-fuels in an EGR equipped micro gas turbine. In: Proceedings of the ASME Turbo Expo
16. Cui YJ, Lin QZ (2012) Realization of flalemess combustion of liquid fuel. In: Advanced Materials Research
17. Ellis W, Lear WE, Singh B, et al (2008) Flameless Combustion of Biofuels in a Semi-Closed Cycle Gas Turbine. In: 46th AIAA Aerospace Sciences Meeting and Exhibit. pp 1–8
18. Torresi M, Camporeale SM, Fortunato B, et al (2010) Diluted combustion in a aerodynamically staged swirled burner fueled by diesel oil. Process Technol a Sustain Energy 1–8
19. Melo MJ, Sousa JMM, Costa M, Levy Y (2009) Experimental investigation of a novel combustor model for gas turbines. J Propuls Power 25:609–617. https://doi.org/10.2514/1.35173
20. Cha CL, Lee HY, Hwang SS (2019) An experiment analysis of MILD combustion with liquid fuel spray in a combustion vessel. J Mech Sci Technol 33:3717–3724. https://doi.org/10.1007/s12206-019-0713-3
21. de Azevedo CG, de Andrade JC, de Souza CF (2015) Flameless compact combustion system for burning hydrous ethanol. Energy. https://doi.org/10.1016/j.energy.2015.07.049
22. de Azevedo CG, de Andrade JC, de Costa F, S, (2013) Experimental valuation diagnostics of hydrous ethanol sprays formed by a blurry injector. J Aerosp Technol Manag. https://doi.org/10.5028/jatm.v5i2.231
23. Gañán-Calvo AM (2005) Enhanced liquid atomization: From flow-focusing to flow-blurring. Appl Phys Lett 1:1. https://doi.org/10.1063/1.1931057
24. Akinyemi OS, Jiang L (2019) Development and combustion characterization of a novel twin-fluid fuel injector in a swirl-stabilized gas turbine burner operating on straight vegetable oil. Exp Therm Fluid Sci. https://doi.org/10.1016/j.expthermflusci.2018.11.014
25. Simmons BM, Agrawal AK (2010) Spray characteristics of a flow-blurring atomizer. At Sprays. https://doi.org/10.1615/AtomizSpr.v20.i9.60
26. Simmons BM, Agrawal AK (2012) Flow blurring atomization for low-emission combustion of liquid biofuels. Combust Sci Technol. https://doi.org/10.1080/00102202.2012.660222
27. Lorenzetto GE, Lefebvre AH (1977) Measurements of drop size on a plain-jet airblast atomizer. AIAA J doi 10(2514/3):60742
28. Lefebvre AH, McDonell VG (2017) Atomization and sprays
29. PETROBRAS DISTRIBUIDORA S.A. (2014) Material Safety Data Sheet (in portuguese) – FISPQ BR0030
30. Edwards T, Maurice LQ (2001) Surrogate mixtures to represent complex aviation and rocket fuels. J Propuls Power doi 10(2514/2):5765
31. Veríssimo AS, Rocha AMA, Costa M (2013) Importance of the inlet air velocity on the establishment of flameless combustion in a laboratory combustor. Exp Therm Fluid Sci 44:75–81. https://doi.org/10.1016/j.expthermflusci.2012.05.015
32. Szegö GG, Dally BB, Nathan GJ (2009) Operational characteristics of a parallel jet MILD combustion burner system. Combust Flame. https://doi.org/10.1016/j.combustflame.2008.08.009
33. Mi J, Li P, Dally BB, Craig RA (2009) Importance of initial momentum rate and air-fuel premixing on moderate or intense low oxygen dilution (MILD) combustion in a recuperative furnace. Energy Fuels. https://doi.org/10.1021/ef900866v
34. Kruse S, Kerschgens B, Berger L et al (2015) Experimental and numerical study of MILD combustion for gas turbine applications. Appl Energy. https://doi.org/10.1016/j.apenergy.2015.03.054
35. Khalil AEE, Gupta AK (2011) Swirling distributed combustion for clean energy conversion in gas turbine applications. Appl Energy 88:3685–3693. https://doi.org/10.1016/j.apenergy.2011.03.048
36. Tuntivoranukul K, Vallikul P, Fungtammasan B et al (2010) Application of the D 2 -law to determine time evolution and burn-out time of evaporating biodiesel spray drop-size distribution. Time 1:59–63
37. Law CK (1982) Recent advances in droplet vaporization and combustion. Prog Energy Combust Sci 8:171–201. https://doi.org/10.1016/0360-1285(82)90011-9
38. Zou C, Cao S, Song Y et al (2014) Characteristics and mechanistic analysis of CO formation in MILD regime with simultaneously diluted and preheated oxidant and fuel. Fuel 130:10–18. https://doi.org/10.1016/j.fuel.2014.04.004
39. Dally BB, Riesmeier E, Peters N (2004) Effect of fuel mixture on moderate and intense low oxygen dilution combustion. Combust Flame. https://doi.org/10.1016/j.combustflame.2004.02.011
40. Tu Y, Su K, Liu H et al (2017) MILD combustion of natural gas using low preheating temperature air in an industrial furnace. Fuel Process Technol 156:72–81. https://doi.org/10.1016/j.fuproc.2016.10.024
41. Cavigiolo A, Galbiati MA, Effuggi A et al (2003) Mild combustion in a laboratory-scale apparatus. Combust Sci Technol 175:1347–1367. https://doi.org/10.1080/00102200302356